Article

Neuron

Layer 5 Circuits in V1 Differentially Control Visuomotor Behavior

Highlights

- Visually cued eyeblink conditioning requires V1, and behavior is modified by arousal
- Activity of corticopontine neurons accurately represents performance
- Corticopontine, but not corticostriatal, output is necessary for performance

Authors

Lan Tang, Michael J. Higley

Correspondence

m.higley@yale.edu

In Brief

Tang and Higley show that corticopontine neurons in visual cortex encode sensory and motor information during a visually cued eyeblink conditioning task and are necessary for performance, highlighting the existence of physically interspersed but functionally segregated networks that control behavior.

Tang & Higley, 2020, Neuron *105*, 1–9
January 22, 2020
https://doi.org/10.1016/j.neuron.2019.10.014

CellPress

Please cite this article in press as: Tang and Higley, Layer 5 Circuits in V1 Differentially Control Visuomotor Behavior, Neuron (2019), https://doi.org/10.1016/j.neuron.2019.10.014

Neuron
Article

Layer 5 Circuits in V1 Differentially Control Visuomotor Behavior

Lan Tang[1] and Michael J. Higley[1,2,*]
[1]Department of Neuroscience, Kavli Institute for Neuroscience, Yale University School of Medicine, New Haven, CT 06510, USA
[2]Lead Contact
*Correspondence: m.higley@yale.edu
https://doi.org/10.1016/j.neuron.2019.10.014

SUMMARY

Neocortical sensory areas are thought to act as distribution hubs, transmitting information about the external environment to downstream areas. Within primary visual cortex, various populations of pyramidal neurons (PNs) send axonal projections to distinct targets, suggesting multiple cellular networks may be independently engaged during behavior. We investigated whether PN subpopulations differentially support visual detection by training mice on a novel eyeblink conditioning task. Applying 2-photon calcium imaging and optogenetic manipulation of anatomically defined PNs, we show that layer 5 corticopontine neurons strongly encode sensory and motor task information and are selectively necessary for performance. Our findings support a model in which target-specific cortical subnetworks form the basis for adaptive behavior by directing relevant information to distinct brain areas. Overall, this work highlights the potential for neurons to form physically interspersed but functionally segregated networks capable of parallel, independent control of perception and behavior.

INTRODUCTION

The role of the mammalian neocortex in generating behavior in response to external sensory information has been investigated in mice across a range of modalities, including visual, auditory, and somatosensory inputs (Glickfeld et al., 2013b; Hong et al., 2018; Kato et al., 2015; Liu et al., 2016; Miyashita and Feldman, 2013; Petruno et al., 2013; Znamenskiy and Zador, 2013). In some cases, inactivation of cortical sensory areas may lead to a disruption of task performance (Glickfeld et al., 2013b; Miyashita and Feldman, 2013; Petruno et al., 2013; Resulaj et al., 2018; Sachidhanandam et al., 2013; Znamenskiy and Zador, 2013). However, recent work has suggested that the detection of sensory cues linked to behavior may not require cortical function, even for optimal performance levels (Hong et al., 2018). A critical element missing from these opposing views is evidence that the activity of cortical neurons carries task-specific information rather than simply providing a non-specific permissive signal to other relevant structures.

One challenge to fully understanding the contribution of the neocortex to behavior is the growing appreciation for the diversity of cell types comprising cortical circuits, with categories determined by molecular and genetic markers, electrophysiological properties, morphology, and projection patterns (Ascoli et al., 2008; Shepherd, 2013; Tasic et al., 2018). Multiple *ex vivo* studies have provided evidence that this diversity extends to patterns of connectivity both within and across layers, suggesting that independent, parallel networks may be common (Anderson et al., 2010; Brown and Hestrin, 2009; Dantzker and Callaway, 2000; Jiang et al., 2015; Morishima et al., 2017). Moreover, investigations of somatosensory and visual cortical areas have demonstrated that projection-specific subtypes of excitatory pyramidal neurons (PNs) can differentially encode information about sensory stimuli (Chen et al., 2013a; Glickfeld et al., 2013a; Kwon et al., 2016; Lur et al., 2016; Yamashita and Petersen, 2016), suggesting segregated streams of information may be directed to various cortical and subcortical targets. However, the functional independence of these physically interspersed local circuits and their engagement during perception and sensorimotor behavior remain unclear.

The question of microcircuit diversity is particularly relevant in layer 5, the principal output from the neocortex to subcortical structures. There, the two primary cell categories comprise neurons that target either the superior colliculus and brainstem or other intratelencephalic areas, including the ipsilateral cortex and striatum (Dembrow et al., 2010; Hattox and Nelson, 2007; Kasper et al., 1994; Larkman and Mason, 1990; Morishima et al., 2011; Shepherd, 2013). We previously showed that, under anesthesia, brainstem-projecting PNs in mouse V1 show higher contrast sensitivity and broader tuning for orientation and spatial frequency in comparison with striatal-projecting cells, suggesting the possibility that these largely non-overlapping populations may form functionally independent microcircuits (Lur et al., 2016). Nevertheless, it is unknown whether such distinct networks might differentially encode and be required for visually guided behavior.

To address this question, we developed a detection task based on visually cued eyeblink conditioning (Freeman and Steinmetz, 2011), requiring the animal to detect a small drifting grating stimulus in order to perform a conditioned blink and avoid a corneal air puff. A number of prior studies have demonstrated a role for both sensory and association cortex in this form of learning (Freeman and Steinmetz, 2011; Siegel et al., 2015;

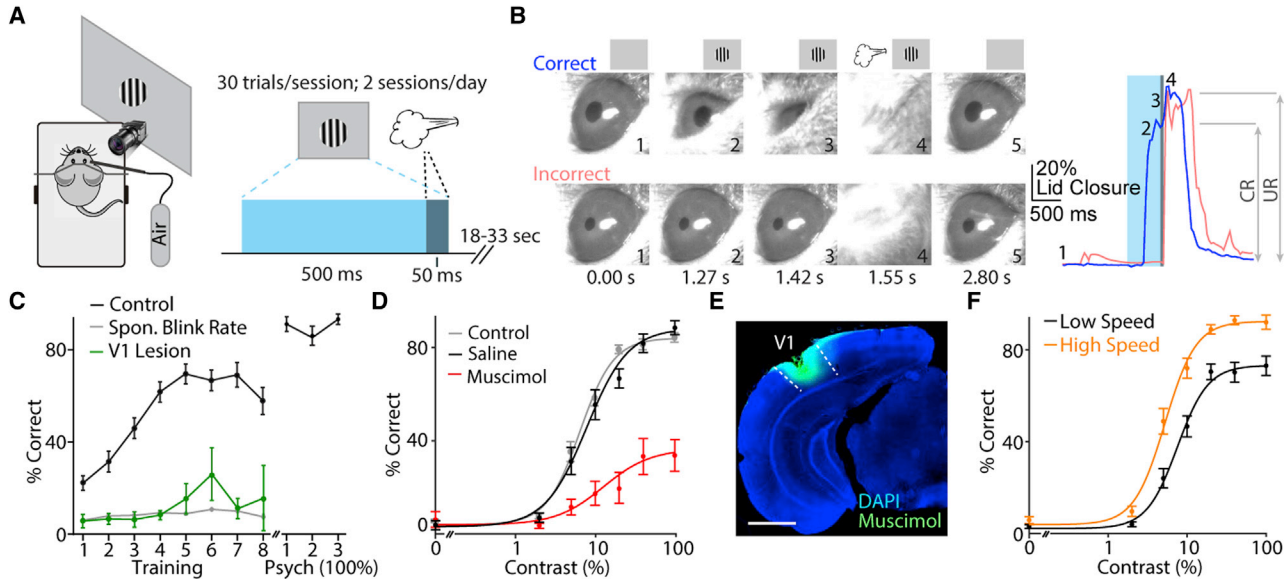

Figure 1. Visual Cortex Is Necessary for Visually Cued Eyeblink Conditioning

(A) Schematic illustration of the behavioral setup (left) and trial structure (right).

(B) Left: example video frames illustrating a correct conditioned blink (upper images) and incorrect unconditioned blink (lower images). Right: time course of lid closure for correct (blue) and incorrect (pink) trials shown in left panel are shown, with timing of individual frames (numbers), visual stimulus (blue bar), and air puff (gray bar) indicated.

(C) Performance over learning for control (black; n = 39 mice) and V1 lesioned (green; n = 8 mice) groups. Dots with error bars represent average ± SEM. Spontaneous blink rate per 450-ms period is shown (gray). Data are shown for training period and psychometric analysis period (100% contrast trials only).

(D) Contrast-dependent performance for all control mice (gray; n = 39 mice) and mice injected with saline (black) and muscimol (red) into V1 15 min prior to testing on alternating days (2 days per treatment; n = 11 mice). Dots with error bars represent average ± SEM. R_{Max}-saline 86.5%; R_{Max}-muscimol 28.2%; $p < 0.0001$; permutation test.

(E) Example showing extent of fluorescent muscimol infusion into V1 (indicated by dashed lines). Scale bar represents 1 mm.

(F) Contrast-dependent performance separated into high (orange) and low (black) locomotion speed trials (n = 39 mice). Dots with error bars represent average ± SEM. R_{Max}-high speed 88.7%; R_{Max}-low speed 71.1%; $p < 0.0001$; permutation test.

Steinmetz et al., 2013). Here, we show that this task requires V1 function for both acquisition and performance of contrast-dependent behavior. Then we apply an intersectional viral labeling strategy to express GCaMP6s in targeted subpopulations of layer 5 PNs and use 2-photon imaging of neuronal activity to show that corticopontine (CPn), but not corticostriatal (CSt), cells robustly encode predictive information about individual trial performance in their stimulus-evoked responses. Finally, we show that optogenetic suppression of CPn activity, but not CSt activity, disrupts task performance. Overall, these data provide strong evidence for cortical representation of visuomotor behavior and demonstrate the functional independence of microcircuits in the primary output layer of V1.

RESULTS

To investigate the functional architecture of mouse primary visual cortex (V1) underlying visual perception, we developed a detection task based on visually cued eyeblink conditioning, in which a mouse, head fixed over a freely moving wheel, must learn to close its eye in response to presentation of a small drifting grating stimulus (500 ms) prior to delivery of an air puff to the ipsilateral cornea (Figures 1A and S1; see STAR Methods; Freeman and Steinmetz, 2011; Heiney et al., 2014). Simultaneous video recording of the eyelid position allowed us to determine correct (presence of conditioned response [CR]) versus incorrect (presence of only unconditioned response [UR]) performance on individual trials (Figures 1A and S1; see STAR Methods). Mice (n = 39) readily learned this task over a few days with a consistently low false alarm rate (spontaneous blinks; Figures 1C and S1). Importantly, V1 lesion contralateral to the visual stimulus in naive mice (n = 8) prevented learning (Figure 1C), suggesting that the cortex is necessary for acquiring this behavior.

During training, the visual stimulus was set to 100% contrast. After mice demonstrated stable performance, the task was changed to present stimuli of varying contrast, allowing us to determine the average psychometric contrast-dependent behavior (Figures 1D and S1). Fitting these data with a hyperbolic ratio function (see STAR Methods) revealed the mean group performance (R_{Max}: 81.2% ± 1.9% correct; c50: 7.8% ± 0.7% contrast; n = 39 mice; Figure 1D). In addition, both CR:UR ratio (response magnitude) and response latency were monotonically modulated by contrast (Figure S1). Unilateral inactivation of V1 using injection of the GABAergic agonist muscimol 15 min prior to testing significantly impaired performance across contrasts (see STAR Methods; R_{Max}-saline: 86.5%, R_{Max}-muscimol: 28.2%, $p < 0.0001$; permutation test; n = 11 mice; Figures 1D

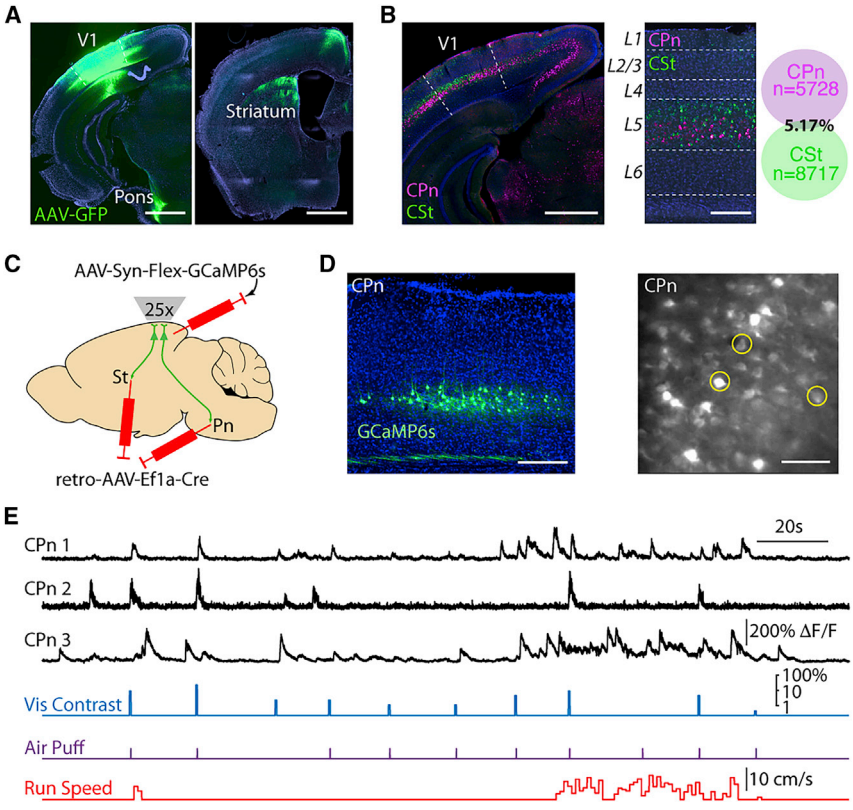

Figure 2. Two-Photon Imaging of Activity in Projection-Specific Layer 5 Subpopulations

(A) Injection of AAV5-hSyn-GFP into V1 (indicated by dashed lines) labels projections in both the ipsilateral pons (left) and ipsilateral dorsal striatum (right). Scale bars represent 1 mm.

(B) Retrograde labeling of corticopontine (CPn) (pink) and corticostriatal (CSt) (green) cells with dual-color cholera toxin subunit B injections into ipsilateral pons or striatum reveals two non-overlapping populations in V1 (indicated by dashed lines) that are mostly limited to layer 5 (left, center). Scale bars represent 200 μm. Co-localization of CPn and CSt neurons is shown (right; n = 3 mice).

(C) Schematic illustrating intersectional viral approach for conditional expression of the calcium indicator GCaMP6s in layer 5 PNs projecting to either the ipsilateral dorsal striatum (St) or pons (Pn).

(D) Left: example *ex vivo* image showing restricted expression of GCaMP6s in layer 5 CPn neurons. Scale bar represents 200 μm. Right: example *in vivo* 2-photon imaging of CPnneurons at 525-μm depth is shown (image averaged over 5 s). Scale bar represents 100 μm.

(E) Example traces showing simultaneous recordings of three CPn neurons from (D), timing of visual stimuli, air puff, and continuous running speed.

and 1E), further suggesting that V1 is necessary for this task. Changes in behavioral state are also known to modulate cortical activity and perception (McGinley et al., 2015a, 2015b; Niell and Stryker, 2010; Polack et al., 2013; Vinck et al., 2015). We monitored locomotion and found that high-speed trials exhibited significantly enhanced performance (R_{Max}-high speed: 88.7%, R_{Max}-low speed: 71.1%, $p < 0.0001$; permutation test; n = 39 mice; Figure 1F). Locomotion was also correlated with larger CR magnitude (Figure S1; Table S1), consistent with state-dependent modulation of cerebellar motor control (Albergaria et al., 2018). Notably, similar results were seen for pupil dilation (Figure S1; Table S1). Overall, these results suggest that visually cued eyeblink conditioning provides a useful approach for investigating V1-dependent behavior.

We next set out to determine how V1 neurons participate in visually cued eyeblink conditioning. Cortical outputs to the lateral pons may serve to direct sensory information to cerebellar structures critical for establishing associations between conditioned and unconditioned stimuli (Freeman and Steinmetz, 2011). Previous work in cats suggested that corticopontine projections arise from multiple visual areas (Brodal, 1972; Glickstein et al., 1972). Using adenoassociated viral (AAV) tracing, we found that mouse V1 sends a strong projection to subcortical areas, including the pons and dorsal striatum (Figure 2A). Retrograde tracing from the pons labeled a subpopulation of layer 5 PNs in V1 as well as secondary visual areas and the retrosplenial cortex (Figure 2B). Consistent with earlier work from our lab (Lur et al., 2016), these CPn cells were largely non-overlapping with co-mingled cells in layer 5 projecting to the ipsilateral dorsal striatum (CSt; Figure 2B). As both pathways have been linked to sensorimotor function (Liu et al., 2016; Znamenskiy and Zador, 2013) and may extract distinct visual features from the environment (Lur et al., 2016), we investigated whether these two populations might be differentially involved in the control of conditioned visuomotor behavior.

To monitor the activity of different layer 5 PNs in task performance, we drove expression of Cre recombinase in either CPn or CSt cells using a retrograde AAV vector (retroAAV-Ef1a-Cre; Tervo et al., 2016) injected into either the pons or striatum. We then drove conditional expression of the genetically encoded calcium indicator GCaMP6s (Chen et al., 2013b) with a second vector (AAV-Syn-Flex-GCaMP6s) injected into ipsilateral V1 (Figure 2C). This approach resulted in selective labeling of the targeted subpopulation, compatible with monitoring neuronal activity in layer 5 of behaving mice via 2-photon microscopy through a chronically implanted cranial window (Figure 2D). Importantly, we previously showed that the relationship between GCaMP6s fluorescence and somatic spiking does not differ between subtypes of layer 5 PNs (Lur et al., 2016).

Neuropil-subtracted fluorescence signals (ΔF/F) were collected and combined across 4– 5 days during the psychometric (varied contrast) phase of the task (Figures 2E and S2). Cells exhibited spontaneous and visually evoked activity, as well as modulation correlated with locomotion (Figures 2E and S3). Consistent with previous reports (Vinck et al., 2015), cells exhibited a short latency response to presentation of the air puff alone (180 ± 9 ms; Figure S3). Additionally, similar to findings in monkeys (Gawne and Martin, 2000), both populations also

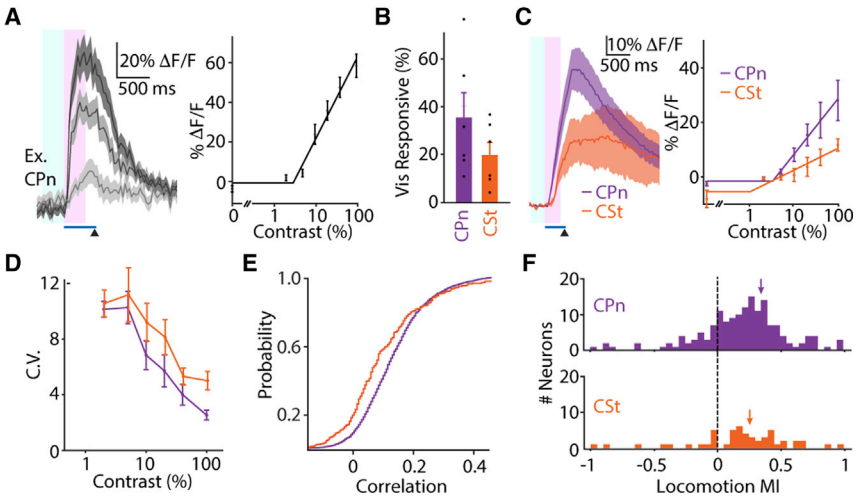

Figure 3. Visually Evoked Activity Varies between Layer 5 Subpopulations

(A) Left: visual responses from an example cell (CPn 1 from Figure 2E) at 5%, 20%, and 100% contrast. Timings of visual stimulus (blue bar) and air puff (arrowhead) are shown. Intervals for measuring baseline activity (light blue window) and visual response magnitude (pink window) are shown. Right: contrast-dependent response magnitudes and rectified linear curve fit for the cell are shown. Lines and shadings represent average ± SEM over trials.

(B) Proportion of visually responsive neurons in CPn (purple; n = 6 mice; n = 159 cells) and CSt (orange; n = 6 mice; n = 51 cells) cohorts. Bars represent average ± SEM over mice. CPn 34.9% ± 10.5%; CSt 19.5% ± 5.5%; p = 0.39; Mann-Whitney U test.

(C) Left: population visual responses at 100% contrast for CPn (purple; n = 6 mice) and CSt (orange; n = 6 mice) cohorts. Lines and shadings represent average ± SEM over animals. Right: population contrast-dependent response magnitudes for CPn and CSt cohorts are shown. Dots with error bars represent average ± SEM across mice. CPn slope 0.20 ± 0.06; CSt slope 0.10 ± 0.02; p = 0.016; n = 6 mice per group; Mann-Whitney U test.

(D) Population contrast-dependent coefficient of variation for CPn and CSt cohorts. Dots with error bars represent average ± SEM across mice. CPn area under the curve (AUC) 29.2 ± 3.3; CSt AUC 37.9 ± 1.4; p = 0.04; n = 6 mice per group; Mann-Whitney U test.

(E) Cumulative distributions of pairwise noise correlations for the two cohorts. CPn, 9,453 pairs, median = 0.114; CSt, 2,145 pairs, median = 0.072; p < 0.0001; Kolmogorov-Smirnov test.

(F) Histograms illustrating the distribution of locomotion modulation index values for the two cohorts. Mean values are indicated by arrows. CPn 0.36 ± 0.07, n = 159 cells; CSt 0.26 ± 0.03, n = 51 cells; p = 0.12; t test.

exhibited responses to spontaneous eyeblinks (299 ± 15 ms; Figure S3), potentially reflecting the brief change in luminance. To avoid contamination of the measured visual response, we quantified the evoked activity as the average signal in the 300-ms window following stimulus onset (prior to the blink response), subtracting the preceding 300-ms baseline period (Figures 3A and S3). Visually responsive neurons (see STAR Methods) exhibited monotonically increasing output with increasing log-transformed visual contrast that was well fit with a rectified linear contrast response function (CRF) (Figure 3A). This approach gave similar results to a sigmoid hyperbolic ratio function and yielded a single slope variable that could be compared across groups (Figure S3; Table S1).

The percentage of visually responsive neurons did not differ significantly between groups (CPn: 34.9% ± 10.5%, 159 neurons, 6 mice; CSt: 19.9% ± 5.5%, 51 neurons, 6 mice; p = 0.39; Mann-Whitney U test; Figure 3B). CPn neurons exhibited significantly larger visual responses than CSt neurons (CPn slope: 0.20 ± 0.06; CSt slope 0.10 ± 0.02; n = 6 mice per group; p = 0.016; Mann-Whitney U test; Figure 3C). CPn neurons also produced more reliable responses, measured as the area under the curve of the contrast-modulated coefficient of variation (CPn AUC: 29.2 ± 3.3, n = 6 mice; CSt AUC: 37.9 ± 1.4, n = 6 mice; p = 0.04; Mann-Whitney U test; Figure 3D). Furthermore, consistent with our previous findings (Lur et al., 2016), the average pairwise noise correlations were greater for CPn versus CSt neurons (p < 0.0001; Kolmogorov-Smirnov test; Figure 3E; Table S1). Finally, both populations were similarly modulated by arousal, with cells in each group exhibiting positive or negative changes in visual responses associated with locomotion (Figure 3F; Table S1). These results suggest that, in mice trained on a conditioned visuomotor task, CPn neurons form a more robust and reliable network for distributing visual signals to subcortical structures.

To determine whether CPn and CSt cells can encode task performance, we first separated visual responses into correct and incorrect trials to look at the average evoked activity. At contrasts near the behavioral threshold (20% contrast), CPn neurons demonstrated a larger average response in correct trials compared to incorrect trials, and CSt neurons exhibited similar responses for both trial outcomes (Figures 4A, 4B, and S4). These results were significant across the range of contrasts (CPn $slope_{Correct}$: 0.16, CPn $slope_{Incorrect}$: 0.10, n = 6 mice, p = 0.0004, permutation test; CSt $slope_{Correct}$: 0.12, CSt $slope_{Incorrect}$: 0.09, n = 6 mice, p = 0.14, permutation test; Figures 4C, 4D, and S4).

We then asked whether the output of the two populations could predict behavior on individual trials. We built a cross-validated logistic regression-based linear model using the population activity of all CPn or CSt neurons to predict the outcome (blink or no blink) for each trial (see STAR Methods). CPn activity reliably predicted psychometric behavioral data across all contrast levels (Figure 4E), whereas CSt activity performed substantially poorer (Figure 4F). We quantified behavioral discriminability (d') (see STAR Methods) for the two populations and found that CPn output was significantly better than CSt output at predicting behavior (CPn d': 0.88 ± 0.12; CSt d': 0.24 ± 0.24; n = 6 mice per group; p = 0.026; Mann-Whitney U test; Figure 4G). These d' values corresponded to area under the receiver-operator curve (ROC) values of 0.70 ± 0.03 versus 0.60 ± 0.05 (n = 6 mice per group; p = 0.03; Mann-Whitney U test). We obtained similar results when we further restricted our analyses to time windows preceding the onset of the

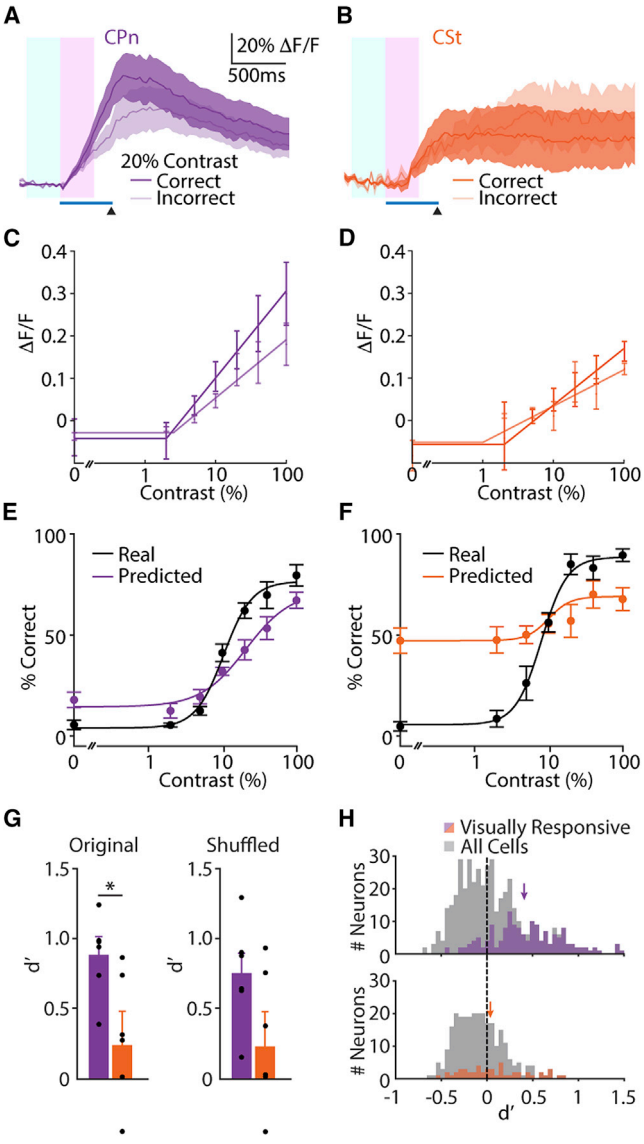

Figure 4. Behavior Is Selectively Encoded by Activity in CPn Neurons

(A and B) Averaged visual responses at 20% contrast for 159 CPn neurons in 6 mice (A) and 51 CSt neurons in 6 mice (B) separated by correct (dark) and incorrect (light) trials. Timing of visual stimulus (blue bar) and air puff (arrowhead) and analysis windows (baseline, light blue; response, pink) are shown. Lines and shadings represent average ± SEM over animals.

(C) Population contrast-dependent response magnitudes for CPn neurons (n = 6 mice) separated by correct (dark) and incorrect (light) trials. Dots and error bars represent average ± SEM over mice. CPn slope-correct 0.16; slope-incorrect 0.10; p = 0.0004; permutation test.

(D) As in (C) for CSt neurons (n = 6 mice). CSt slope-correct 0.12; slope-incorrect 0.09; p = 0.14; permutation test.

(E and F) Real (black) and predicted (purple/orange) contrast-dependent behavior based on CPn responses (E) and CSt responses (F). Dots and error bars represent average ± SEM over mice.

(G) Discriminability (d') for the ensemble decoders using CPn (purple; n = 6 mice) or CSt (orange; n = 6 mice) responses on original data (acquired simultaneously; left) or trial shuffled data (right). Bars represent average ± SEM over mice. CPn original trials d' 0.88 ± 0.12, CSt original trials d' 0.24 ± 0.24; p = 0.026, Mann-Whitney U test. CPn shuffled trials d' 0.75 ± 0.16, CSt shuffled trials d' 0.22 ± 0.25; p = 0.18, Mann-Whitney U test.

(H) Histograms illustrating the distribution of d' values for single visually responsive CPn (purple, top) or CSt (orange, bottom) neurons, mean values indicated by arrows. CPn average d' 0.43 ± 0.03, chance d' −0.01 ± 0.001, n = 159 cells; p < 0.0001, one-sided t test. CSt average d' 0.09 ± 0.05, chance d' −0.02 ± 0.002, n = 51 cells; p = 0.088, one-sided t test. CPn versus CSt, p < 0.0001, t test. d' values for all CPn (top) and CSt (bottom) neurons are shown in gray.

eyeblink on each trial (see STAR Methods; CPn d': 0.90 ± 0.10; CSt d': 0.29 ± 0.23; n = 6 mice per group; p = 0.002; Mann-Whitney U test). Finally, to examine the role of neuronal correlations in behavioral encoding, we shuffled individual trials and repeated the analyses (see STAR Methods). This comparison revealed a small reduction in d' values for both groups and eliminated the significant difference between the populations (CPn d': 0.74 ± 0.16; CSt d': 0.22 ± 0.25; n = 6 mice per group; p = 0.18; Mann-Whitney U test; Figure 4G).

Behavior was also encoded, on average, by the output of single CPn neurons but not single CSt neurons (average CPn d': 0.42 ± 0.03; n = 159 cells; p < 0.0001 versus chance; one-sided t test; Figure 4H; CSt d':0.09 ± 0.05; n = 51 cells; p = 0.09 versus chance; one-sided t test). These data yielded a significant animal-wise difference between CPn and CSt cohorts (CPn versus CSt; n = 6 mice per group; p = 0.015; Mann-Whitney U test; Figure 4H; Table S1).

The preceding results indicate that linear modeling based on the activity of CPn neurons is better able to predict individual trial performance versus CSt activity. We therefore wanted to determine whether the output of either population was necessary for normal task performance. We again used a retrograde AAV vector to express Cre recombinase in either of the two groups and a second AAV to conditionally express the optogenetic suppressor ArchT in V1 (Figures 5A and 5B; Chow et al., 2010). This approach produced a similar low density of infected cells (~7.5% of all layer 5 neurons) in each group (Figure S5; Table S1). Mice were also implanted chronically with a guide cannula to enable placement of a fiber optic coupled to a 594-nm laser directly over V1 during the session.

During the psychometric performance phase of training, a 3-s light pulse (120–160 mW/mm^2 at the sample) was delivered to V1 on randomly interleaved trials, beginning 2 s before visual stimulus onset. This experimental approach is expected to robustly suppress cortical spiking *in vivo* (Li et al., 2019). Moreover, we carried out *ex vivo* recordings to compare the sensitivity of CPn and CSt cells to optical suppression, finding no significant differences between the groups (Figure S5; Table S1). Optogenetic inhibition of CPn neurons significantly suppressed behavior (R_{Max} $Laser_{Off}$: 80.2%; R_{Max} $Laser_{On}$: 60.5%; n = 11 mice; p < 0.0001; permutation test; Figure 5C). In contrast, inhibition of CSt neurons had no effect (R_{Max} $Laser_{Off}$: 77.7%; R_{Max} $Laser_{On}$: 79.3%; n = 12 mice; p = 0.24; permutation test; Figure 5D). Importantly, optogenetic inhibition of either population did not directly interfere with motor ability, as unconditioned blink magnitudes were unaffected (Figure S5; Table S1). These findings demonstrate that activity in CPn neurons not only

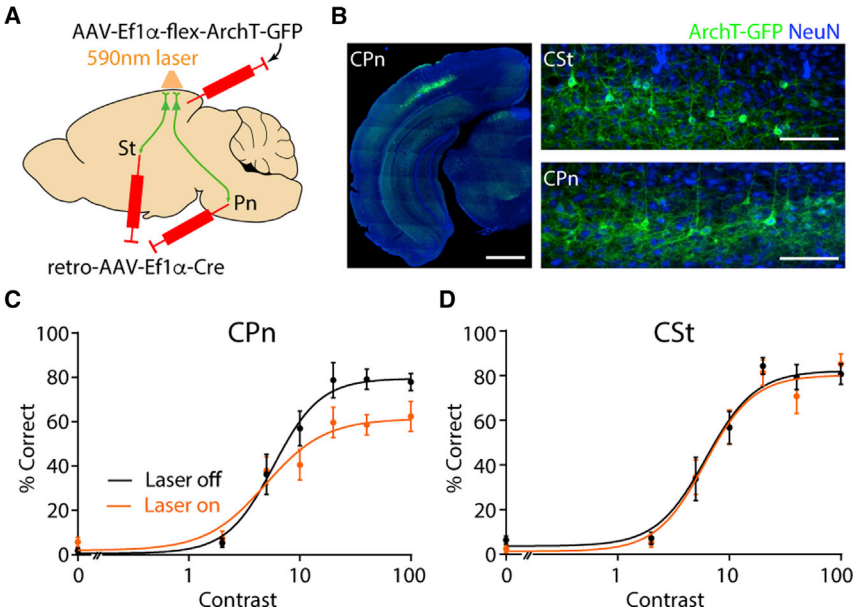

Figure 5. Optogenetic Suppression of CPn Activity Disrupts Behavioral Performance

(A) Schematic illustrating intersectional viral approach for conditional expression of ArchT-GFP in either CPn or CSt neurons.

(B) Left: example *ex vivo* image showing restricted expression of ArchT-GFP in V1 CPn neurons. Scale bar represents 1 mm. Right: CPn (bottom image) and CSt (top image) neurons are similarly labeled. Scale bars represent 100 μm.

(C) Contrast-dependent performance for CPn cohort (n = 11 mice) separated by trials with laser off (black) or on (orange). Dots with error bars represent average ± SEM over mice, combining 3 to 4 days of behavior. R_{Max} $Laser_{Off}$ 80.2%; R_{Max} $Laser_{On}$ 60.5%; $p < 0.0001$; permutation test.

(D) As in (C) for CSt cohort (n = 12 mice). R_{Max} $Laser_{Off}$ 79.3%; R_{Max} $Laser_{On}$ 77.7%; $p = 0.325$; permutation test.

encodes individual trial outcome but is required for optimal task performance.

DISCUSSION

In the present study, we developed a paradigm for probing the role of cortical microcircuits in visually guided behavior. Our results indicate that mouse V1 is necessary for learning and performing a visuomotor task that requires perception of a small contrast-modulated stimulus to produce a conditioned eyeblink response. This finding is consistent with earlier work showing a role for both association and sensory areas of the neocortex as well as the hippocampus and amygdala in eyeblink conditioning (Freeman and Steinmetz, 2011; Siegel et al., 2015; Steinmetz et al., 2013). Both CPn and CSt cells responded to visual input, with the former exhibiting more robust responses, on average, potentially reflecting their broader orientation and spatial frequency tuning (Lur et al., 2016). Interestingly, both populations also responded transiently to air puffs alone and spontaneous eyeblinks, consistent with earlier work in rodents and primates (Gawne and Martin, 2000; Vinck et al., 2015). Moreover, CPn (but not CSt) layer 5 PNs significantly encoded behavioral outcome using a linear model, and their activity was necessary for normal task performance. Notably, CPn cells also exhibited stronger pairwise ''noise'' correlations across visual responses. Removal of within trial correlations via shuffling eliminated the significant difference between CPn and CSt encoding, suggesting that the correlational structure of layer 5 activity may enhance behavioral representations in this task. Overall, these findings support a model in which corticopontine projections provide an instructive di-synaptic relay of visual signals to the cerebellum, where synaptic plasticity is thought to drive the association between conditioned and unconditioned stimuli (Albergaria et al., 2018; Christian and Thompson, 2003; Freeman and Steinmetz, 2011). Thus, cortical neurons are organized into physically interspersed networks that can differentially participate in sensory-guided behavior.

Layer 5 PNs have long been recognized as a heterogeneous population based on morphology, electrophysiological properties, genetic markers, and projection targets (Hattox and Nelson, 2007; Kasper et al., 1994; Larkman and Mason, 1990; Lur et al., 2016). Indeed, multiple studies confirm the almost complete anatomical segregation of ''pyramidal tract'' and ''intratelencephalic'' populations, corresponding to our CPn and CSt cells (Kim et al., 2015; Larkman and Mason, 1990; Shepherd, 2013). Recent work from our lab and others suggests differential representation of visual stimuli, with brainstem-projecting PNs exhibiting broader orientation and spatial frequency tuning (Kim et al., 2015; Lur et al., 2016). Synaptic connectivity of subgroups of layer 5 PNs with other PNs as well as with local interneurons may also differ, suggesting a basis for these distinct functional properties (Brown and Hestrin, 2009; Morishima et al., 2017). Importantly, both populations most likely send projections to additional areas, with CPn cells also targeting the superior colliculus and CPn and CSt cells targeting other cortical regions (Shepherd, 2013). The possibility that different networks of cortical PNs, organized around common projection targets, might transmit distinct streams of behaviorally relevant information has been suggested for visual, somatosensory, and auditory areas (Chen et al., 2013a; Kwon et al., 2016; Liu et al., 2016; Yamashita and Petersen, 2016; Znamenskiy and Zador, 2013). Interestingly, modulation of corticostriatal activity was shown to alter behavioral output in an auditory discrimination task (Znamenskiy and Zador, 2013), suggesting that layer 5 subnetworks may be differentially engaged by sensory inputs on the basis of current expectations or environmental demands. It will be very interesting to determine whether sensory representations in various cortical populations are plastic in response to passive experience versus task learning.

Recent studies have called into question the function of the neocortex in learning and performance of basic sensory and motor tasks (Hong et al., 2018; Kawai et al., 2015). Here, we find that visually cued eyeblink conditioning is disrupted by V1 lesion, acute V1 inactivation, or selective optogenetic suppression of CPn cells, indicating a necessary role for cortical activity. Nevertheless, muscimol infusion into V1 did not completely abolish performance, suggesting that other subcortical structures, such as the thalamus and superior colliculus, may also relay visual information to the pons that is capable of supporting behavior. The relatively modest optogenetic behavioral suppression is likely a reflection of the small percentage of ArchT-expressing neurons, given the low efficiency of dual-AAV intersectional infection. Our *ex vivo* recordings indicate that both CPn and CSt cells are similarly inhibited by photoactivation of ArchT, making it unlikely that differential sensitivity to the opsin explains our behavioral data. Moreover, a recent study demonstrated robust ArchT-mediated suppression of cortical activity in layer 5 *in vivo* (Li et al., 2019). The observation that the effect of optogenetic suppression is greater at higher contrast levels suggests that CPn activity may regulate the response gain rather than the sensitivity of visual processing (e.g., multiplicative scaling versus a lateral shift in the contrast response function). It will be interesting to expand these results by examining the role of layer 5 circuits in a variety of behavioral paradigms. Beyond inactivation studies, our imaging data demonstrate that the activity of cortical neurons encodes trial-by-trial performance, arguing that V1 is not simply providing a non-specific permissive signal to other brain structures. The reasons for discrepancies in the literature regarding cortical necessity are unclear, though the aversive conditioning nature of our task and the specific involvement of brainstem-projecting PNs may distinguish our results from those obtained with appetitive, operant behavior. Indeed, our results indicate that caution is necessary when attempting to generalize conclusions from a single study to other behavioral paradigms.

Our results are also consistent with studies demonstrating that behavioral state can modulate perceptual ability, neuronal activity, and motor learning in mice (Albergaria et al., 2018; McGinley et al., 2015a; Vinck et al., 2015). The cellular mechanisms of this effect remain unclear, with potential contributions from neuromodulatory systems (Constantinople and Bruno, 2011; Pinto et al., 2013; Polack et al., 2013) and top-down feedback from other cortical regions and engagement of local inhibitory circuits (Fu et al., 2014; Zhang et al., 2014). Interestingly, our imaging data indicate that different layer 5 PNs exhibit either increases or decreases in activity during arousal, suggesting that the links between internal state, cortical signaling, and behavioral output are not straightforward.

In conclusion, our study demonstrates that layer 5 CPn neurons play a key role in the representation of visual information that is necessary for performing a conditioned motor behavior. This work supports the projection-specific parcellation of cortical projection neurons and provides strong evidence for the functional segregation of cortical microcircuits, even within a single layer. The formation and preservation of these distinct but physically interspersed networks are likely to be critical processes during cortical development, and loss of this specificity may ultimately contribute to abnormal sensorimotor behaviors associated with synaptic alterations in neuropsychiatric disorders.

STAR★METHODS

Detailed methods are provided in the online version of this paper and include the following:

- KEY RESOURCES TABLE
- LEAD CONTACT AND MATERIALS AVAILABILITY
- EXPERIMENTAL MODEL AND SUBJECT DETAILS
- METHOD DETAILS
  - Transcranial injection of retrograde tracer and virus
  - Histology
  - Cannulation, head-posting, and window implantation
  - Visual stimulation
  - Behavioral setup
  - Muscimol inactivation
  - Induced pupil dilation
  - Optogenetic suppression of cortical activity
  - Behavioral Training
  - Calcium imaging
  - *Ex vivo* electrophysiology
- QUANTIFICATION AND STATISTICAL ANALYSIS
  - Behavioral analysis and statistics
  - Imaging analysis and statistics
- DATA AND CODE AVAILABILITY

SUPPLEMENTAL INFORMATION

Supplemental Information can be found online at https://doi.org/10.1016/j.neuron.2019.10.014.

ACKNOWLEDGMENTS

The authors wish to thank Dr. Daeyeol Lee for help with statistical analyses. We also thank Dr. Jessica A. Cardin and members of the Cardin and Higley laboratories for helpful discussions during the preparation of this manuscript. These studies were funded by grants from the NIH (R01 MH099045, R01 MH113852, and P30 EY026878) and the Brain Research Foundation (Fay/Frank Seed Grant).

AUTHOR CONTRIBUTIONS

L.T. and M.J.H. designed the research, performed the experiments, analyzed the data, and wrote the paper.

DECLARATION OF INTERESTS

The authors declare no competing interests.

Received: April 1, 2019
Revised: September 3, 2019
Accepted: October 7, 2019
Published: November 19, 2019

REFERENCES

Albergaria, C., Silva, N.T., Pritchett, D.L., and Carey, M.R. (2018). Locomotor activity modulates associative learning in mouse cerebellum. Nat. Neurosci. *21*, 725–735.

Anderson, C.T., Sheets, P.L., Kiritani, T., and Shepherd, G.M. (2010). Sublayer-specific microcircuits of corticospinal and corticostriatal neurons in motor cortex. Nat. Neurosci. *13*, 739–744.

Ascoli, G.A., Alonso-Nanclares, L., Anderson, S.A., Barrionuevo, G., Benavides-Piccione, R., Burkhalter, A., Buzsáki, G., Cauli, B., Defelipe, J., Fairén, A., et al.; Petilla Interneuron Nomenclature Group (2008). Petilla terminology: nomenclature of features of GABAergic interneurons of the cerebral cortex. Nat. Rev. Neurosci. *9*, 557–568.

Brodal, P. (1972). The corticopontine projection from the visual cortex in the cat. I. The total projection and the projection from area 17. Brain Res. *39*, 297–317.

Brown, S.P., and Hestrin, S. (2009). Intracortical circuits of pyramidal neurons reflect their long-range axonal targets. Nature *457*, 1133–1136.

Chen, J.L., Carta, S., Soldado-Magraner, J., Schneider, B.L., and Helmchen, F. (2013a). Behaviour-dependent recruitment of long-range projection neurons in somatosensory cortex. Nature *499*, 336–340.

Chen, T.W., Wardill, T.J., Sun, Y., Pulver, S.R., Renninger, S.L., Baohan, A., Schreiter, E.R., Kerr, R.A., Orger, M.B., Jayaraman, V., et al. (2013b). Ultrasensitive fluorescent proteins for imaging neuronal activity. Nature *499*, 295–300.

Chow, B.Y., Han, X., Dobry, A.S., Qian, X., Chuong, A.S., Li, M., Henninger, M.A., Belfort, G.M., Lin, Y., Monahan, P.E., and Boyden, E.S. (2010). High-performance genetically targetable optical neural silencing by light-driven proton pumps. Nature *463*, 98–102.

Christian, K.M., and Thompson, R.F. (2003). Neural substrates of eyeblink conditioning: acquisition and retention. Learn. Mem. *10*, 427–455.

Constantinople, C.M., and Bruno, R.M. (2011). Effects and mechanisms of wakefulness on local cortical networks. Neuron *69*, 1061–1068.

Dantzker, J.L., and Callaway, E.M. (2000). Laminar sources of synaptic input to cortical inhibitory interneurons and pyramidal neurons. Nat. Neurosci. *3*, 701–707.

Dembrow, N.C., Chitwood, R.A., and Johnston, D. (2010). Projection-specific neuromodulation of medial prefrontal cortex neurons. J. Neurosci. *30*, 16922–16937.

Dubbs, A., Guevara, J., and Yuste, R. (2016). moco: fast motion correction for calcium imaging. Front. Neuroinform. *10*, 6.

Freeman, J.H., and Steinmetz, A.B. (2011). Neural circuitry and plasticity mechanisms underlying delay eyeblink conditioning. Learn. Mem. *18*, 666–677.

Fu, Y., Tucciarone, J.M., Espinosa, J.S., Sheng, N., Darcy, D.P., Nicoll, R.A., Huang, Z.J., and Stryker, M.P. (2014). A cortical circuit for gain control by behavioral state. Cell *156*, 1139–1152.

Gawne, T.J., and Martin, J.M. (2000). Activity of primate V1 cortical neurons during blinks. J. Neurophysiol. *84*, 2691–2694.

Glickfeld, L.L., Andermann, M.L., Bonin, V., and Reid, R.C. (2013a). Cortico-cortical projections in mouse visual cortex are functionally target specific. Nat. Neurosci. *16*, 219–226.

Glickfeld, L.L., Histed, M.H., and Maunsell, J.H. (2013b). Mouse primary visual cortex is used to detect both orientation and contrast changes. J. Neurosci. *33*, 19416–19422.

Glickstein, M., Stein, J., and King, R.A. (1972). Visual input to the pontine nuclei. Science *178*, 1110–1111.

Hattox, A.M., and Nelson, S.B. (2007). Layer V neurons in mouse cortex projecting to different targets have distinct physiological properties. J. Neurophysiol. *98*, 3330–3340.

Heiney, S.A., Wohl, M.P., Chettih, S.N., Ruffolo, L.I., and Medina, J.F. (2014). Cerebellar-dependent expression of motor learning during eyeblink conditioning in head-fixed mice. J. Neurosci. *34*, 14845–14853.

Hong, Y.K., Lacefield, C.O., Rodgers, C.C., and Bruno, R.M. (2018). Sensation, movement and learning in the absence of barrel cortex. Nature *561*, 542–546.

Jiang, X., Shen, S., Cadwell, C.R., Berens, P., Sinz, F., Ecker, A.S., Patel, S., and Tolias, A.S. (2015). Principles of connectivity among morphologically defined cell types in adult neocortex. Science *350*, aac9462.

Kasper, E.M., Larkman, A.U., Lübke, J., and Blakemore, C. (1994). Pyramidal neurons in layer 5 of the rat visual cortex. I. Correlation among cell morphology, intrinsic electrophysiological properties, and axon targets. J. Comp. Neurol. *339*, 459–474.

Kato, H.K., Gillet, S.N., and Isaacson, J.S. (2015). Flexible sensory representations in auditory cortex driven by behavioral relevance. Neuron *88*, 1027–1039.

Kawai, R., Markman, T., Poddar, R., Ko, R., Fantana, A.L., Dhawale, A.K., Kampff, A.R., and Ölveczky, B.P. (2015). Motor cortex is required for learning but not for executing a motor skill. Neuron *86*, 800–812.

Kim, E.J., Juavinett, A.L., Kyubwa, E.M., Jacobs, M.W., and Callaway, E.M. (2015). Three types of cortical layer 5 neurons that differ in brain-wide connectivity and function. Neuron *88*, 1253–1267.

Kwon, S.E., Yang, H., Minamisawa, G., and O'Connor, D.H. (2016). Sensory and decision-related activity propagate in a cortical feedback loop during touch perception. Nat. Neurosci. *19*, 1243–1249.

Larkman, A., and Mason, A. (1990). Correlations between morphology and electrophysiology of pyramidal neurons in slices of rat visual cortex. I. Establishment of cell classes. J. Neurosci. *10*, 1407–1414.

Li, N., Chen, S., Guo, Z.V., Chen, H., Huo, Y., Inagaki, H.K., Davis, C., Hansel, D., Guo, C., and Svoboda, K. (2019). Spatiotemporal limits of optogenetic manipulations in cortical circuits. bioRxiv. https://doi.org/10.1101/642215.

Liu, B.H., Huberman, A.D., and Scanziani, M. (2016). Cortico-fugal output from visual cortex promotes plasticity of innate motor behaviour. Nature *538*, 383–387.

Lur, G., Vinck, M.A., Tang, L., Cardin, J.A., and Higley, M.J. (2016). Projection-specific visual feature encoding by layer 5 cortical subnetworks. Cell Rep. *14*, 2538–2545.

McGinley, M.J., David, S.V., and McCormick, D.A. (2015a). Cortical membrane potential signature of optimal states for sensory signal detection. Neuron *87*, 179–192.

McGinley, M.J., Vinck, M., Reimer, J., Batista-Brito, R., Zagha, E., Cadwell, C.R., Tolias, A.S., Cardin, J.A., and McCormick, D.A. (2015b). Waking state: rapid variations modulate neural and behavioral responses. Neuron *87*, 1143–1161.

Miyashita, T., and Feldman, D.E. (2013). Behavioral detection of passive whisker stimuli requires somatosensory cortex. Cereb. Cortex *23*, 1655–1662.

Morishima, M., Morita, K., Kubota, Y., and Kawaguchi, Y. (2011). Highly differentiated projection-specific cortical subnetworks. J. Neurosci. *31*, 10380–10391.

Morishima, M., Kobayashi, K., Kato, S., Kobayashi, K., and Kawaguchi, Y. (2017). Segregated excitatory-inhibitory recurrent subnetworks in layer 5 of the rat frontal cortex. Cereb. Cortex *27*, 5846–5857.

Niell, C.M., and Stryker, M.P. (2010). Modulation of visual responses by behavioral state in mouse visual cortex. Neuron *65*, 472–479.

Petruno, S.K., Clark, R.E., and Reinagel, P. (2013). Evidence that primary visual cortex is required for image, orientation, and motion discrimination by rats. PLoS ONE *8*, e56543.

Pinto, L., Goard, M.J., Estandian, D., Xu, M., Kwan, A.C., Lee, S.H., Harrison, T.C., Feng, G., and Dan, Y. (2013). Fast modulation of visual perception by basal forebrain cholinergic neurons. Nat. Neurosci. *16*, 1857–1863.

Polack, P.O., Friedman, J., and Golshani, P. (2013). Cellular mechanisms of brain state-dependent gain modulation in visual cortex. Nat. Neurosci. *16*, 1331–1339.

Pologruto, T.A., Sabatini, B.L., and Svoboda, K. (2003). ScanImage: flexible software for operating laser scanning microscopes. Biomed. Eng. Online *2*, 13.

Resulaj, A., Ruediger, S., Olsen, S.R., and Scanziani, M. (2018). First spikes in visual cortex enable perceptual discrimination. eLife *7*, e34044.

Sachidhanandam, S., Sreenivasan, V., Kyriakatos, A., Kremer, Y., and Petersen, C.C. (2013). Membrane potential correlates of sensory perception in mouse barrel cortex. Nat. Neurosci. *16*, 1671–1677.

Shepherd, G.M. (2013). Corticostriatal connectivity and its role in disease. Nat. Rev. Neurosci. *14*, 278–291.

Siegel, J.J., Taylor, W., Gray, R., Kalmbach, B., Zemelman, B.V., Desai, N.S., Johnston, D., and Chitwood, R.A. (2015). Trace eyeblink conditioning in mice is dependent upon the dorsal medial prefrontal cortex, cerebellum, and amygdala: behavioral characterization and functional circuitry. eNeuro *2*, ENEURO.0051-14.2015.

Steinmetz, A.B., Harmon, T.C., and Freeman, J.H. (2013). Visual cortical contributions to associative cerebellar learning. Neurobiol. Learn. Mem. *104*, 103–109.

Tasic, B., Yao, Z., Graybuck, L.T., Smith, K.A., Nguyen, T.N., Bertagnolli, D., Goldy, J., Garren, E., Economo, M.N., Viswanathan, S., et al. (2018). Shared and distinct transcriptomic cell types across neocortical areas. Nature *563*, 72–78.

Tervo, D.G., Hwang, B.Y., Viswanathan, S., Gaj, T., Lavzin, M., Ritola, K.D., Lindo, S., Michael, S., Kuleshova, E., Ojala, D., et al. (2016). A designer AAV variant permits efficient retrograde access to projection neurons. Neuron *92*, 372–382.

Vinck, M., Batista-Brito, R., Knoblich, U., and Cardin, J.A. (2015). Arousal and locomotion make distinct contributions to cortical activity patterns and visual encoding. Neuron *86*, 740–754.

Yamashita, T., and Petersen, C.Ch. (2016). Target-specific membrane potential dynamics of neocortical projection neurons during goal-directed behavior. eLife *5*, e15798.

Zhang, S., Xu, M., Kamigaki, T., Hoang Do, J.P., Chang, W.C., Jenvay, S., Miyamichi, K., Luo, L., and Dan, Y. (2014). Selective attention. Long-range and local circuits for top-down modulation of visual cortex processing. Science *345*, 660–665.

Znamenskiy, P., and Zador, A.M. (2013). Corticostriatal neurons in auditory cortex drive decisions during auditory discrimination. Nature *497*, 482–485.

STAR★METHODS

KEY RESOURCES TABLE

REAGENT or RESOURCE	SOURCE	IDENTIFIER
Antibodies		
Rabbit-anti-mouse NeuN	Invitrogen	Cat#711054
Bacterial and Virus Strains		
AAV5-Syn-FLEX-GCaMP6s-WPRE-SV40	Chen et al., 2013b	Addgene Cat#100845
AAV5-CAG-FLEX-ArchT-GFP	Chow et al., 2010	UNC Vector Core"AAV5-CAG-FLEX-ArchT-GFP"
Chemicals, Peptides, and Recombinant Proteins		
Alexa fluor-conjugated cholera toxin subunit B	Thermo Fisher	Cat#C22841 Cat#C22842
Bodipy-conjugated muscimol	Thermo-Fisher	Cat#M23400
Experimental Models: Organisms/Strains		
c57 Bl/6 mice	Envigo	Catalog specified as "C57BL/6 inbred mice"
Software and Algorithms		
ImageJ Moco algorithm	Dubbs et al., 2016	https://github.com/NTCColumbia/moco
MATLAB	The Mathworks	Version 2018a, Statistics and Machine Learning Toolbox, https://www.mathworks.com/products/statistics.html

LEAD CONTACT AND MATERIALS AVAILABILITY

Further information and requests for resources and reagents should be directed to and will be fulfilled by the Lead Contact, Dr. Michael J. Higley (m.higley@yale.edu). This study did not generate new unique reagents.

EXPERIMENTAL MODEL AND SUBJECT DETAILS

All animal handling was performed in accordance with the Yale Institutional Animal Care and Use Committee and federal guidelines. Wild-type C57/bl6 male mice were obtained from Envigo and group housed in standard cages on a 12h light-dark cycle.

METHOD DETAILS

Transcranial injection of retrograde tracer and virus

All surgical procedures were carried out in juvenile mice (P22-28 for viral injection, P30-40 for cholera toxin labeling) under isoflurane anesthesia. For retrograde labeling of layer 5 PNs, 100 nL of cholera toxin subunit B (CTB)-Alexa Fluor-555 or CTB-Alexa Fluor-488 (ThermoFisher) was injected via glass micropipette into the lateral pons (AP: −3.1, ML: 1.2, DV: 4.7 relative to Bregma) or dorsal striatum (AP: 0.5, ML: 1.7, DV: 1.8), respectively. To express either GCaMP6s or ArchT-GFP in specific layer 5 PN populations, 700 nL of retro-AAV-Ef1α-Cre (Addgene) was injected into either the pons or striatum. A second 700 nL injection of AAV5-hSyn-Flex-GCaMP6s (Addgene) or AAV5-Cag-Flex-ArchT-GFP (UNC Vector Core) was made into V1 (AP: −3.5, ML: 2.5, DV: 0.45).

Histology

Ten days after CTB injection or at the conclusion of behavioral experiments, mice under isoflurane anesthesia were perfused transcardially with phosphate buffer (PB) followed by 4% paraformaldehyde (PFA) in (PB). Brains were post-fixed in 4% PFA overnight at 4°C. 40 μm-thick coronal sections containing the primary visual cortex were cut on a vibratome (Leica VT1000) and washed in PB.

For CTB-injected tissue, slices mounted on glass microscope slides and coverslipped with DAPI-containing medium (Prolong, Invitrogen). For NeuN staining on ArchT-GFP-expressing tissue, slices were pretreated in blocking solution (2% BSA, 10% NGS, 0.5% Triton X-100 in PB) for 4 hours followed by incubation in primary antibody (rabbit anti-mouse NeuN, Invitrogen) for 24 hours at 4°C. Slices were then incubated in secondary antibody (goat anti-rabbit-Alexa Fluor 594, Invitrogen) for 2 hours at room temperature and mounted on glass slides.

Slices were imaged on an upright Olympus BX53 fluorescent microscope. A rectangular region of V1 layer 5 (600 μm in width, 350-550 μm in depth from pia) was cropped from the image of each section. For CTB retrograde tracing, a rectangular region of V1 layer 5 (600 μm width, 350-550 μm depth from pial surface) was collected. Labeled cells in each channel were identified and counted using

ImageJ. For estimating ArchT-GFP-expression, we used CellProfiler to expand NeuN-identified nuclei by 2 pixels to estimate somatic area. Neurons were classified as ArchT-GFP-positive if > 60% of soma pixels displayed GFP fluorescence.

Cannulation, head-posting, and window implantation

Mice were anesthetized with isoflurane, the scalp was resected, and a small craniotomy was made over V1. For acute inactivation experiments, a guide cannula (26 gauge, Plastics One) was lowered to the brain surface. For optogenetic experiments, a larger guide cannula (21 gauge, Plastics One) was used. The cannula was secured via two screws set into the skull and dental cement (Metabond, Parkell). For lesion experiments, a similar procedure was used, and V1 was surgically resected using a small metal probe. A custom titanium head-post was then fixed to the skull using dental cement. A blocking stylus was placed in the cannula to prevent contamination. For imaging experiments, a ~4 mm square craniotomy was made over left V1. A bilayer imaging window consisting of a 5x5mm glass coverslip bonded to a 3.5x3.5 mm inner glass using ultraviolet-curing adhesive (Norland Products) was inserted in the craniotomy and secured to the skull with Metabond.

Visual stimulation

Sinusoidal drifting gratings were generated using Psychtoolbox-3 in MATLAB and presented on a gamma-calibrated LCD monitor (17 inches) with a spatial resolution of 1280x960, frame rate of 60 Hz, and mean luminance of 45 cd/m^2. Unilateral stimuli had a 20° visual angle, temporal frequency of 2 Hz, spatial frequency of 0.04 cycles per degree, and orientation of 180°. During the training phase, visual stimuli were set to 100% contrast. During psychometric testing, contrast varied (0%, 2%, 5%, 10%, 20%, 40%, 100%) pseudorandomly. For non-imaging experiments, stimuli were presented in the center of the LCD screen. For calcium imaging experiments, the stimulus was fixed in one of nine 3x3 sub-regions that evoked the largest population response in the field of view.

Behavioral setup

The mouse was head-fixed on a freely moving wheel (15 cm diameter) in a darkened and sound-attenuating chamber. The LCD screen was positioned on the right side at a distance of 22 cm and normal to the right eye. Timing of visual stimuli was recorded using a photo-diode that detected a small luminance signal in the corner of the screen. Brief air puffs (10-12 psi) were generated with a compressed air tank coupled to a solenoid (Clark Solutions). The air puff was directed to the right cornea using a 14-gauge stainless steel cannula positioned ~5 mm from the eye. Timing of the air puff was coordinated with the visual stimulus using custom-written MATLAB codes through a NI-DAQmx board (PCIe-6315, National Instruments) at a sampling rate of 5 kHz. To monitor locomotion, a magnetic angle sensor (Digikey) was attached to the shaft of the wheel. Eyelid closure and pupil diameter were continuously recorded using a monochromatic CMOS camera (PointGrey FlyCapture3) at a frame rate of 33 fps. An infrared LED array was directed toward the animal's to illuminate the eye. All signals, including the timing of the visual stimuli, the air puffs, the wheel position, and video frame ticks were digitized (5 kHz) and recorded through the NI-DAQmx board for non-imaging experiments. For calcium imaging experiments, all signals as well as the microscope resonant scanner frame ticks were digitized (5 kHz) and collected through a Power 1401 (CED) acquisition board using Spike 2 software.

Muscimol inactivation

Saline solution consisted of artificial cerebrospinal fluid (ACSF) adjusted to pH of 7.4. Muscimol (1 μg/μl, Sigma) or bodipy-tagged muscimol (1 μg/μl, Thermo-Fisher, final day only) was dissolved in ACSF. At the conclusion of the final behavioral day, mice were perfused and their brains sectioned to validate the infusion site and extent. On alternating days, either saline or muscimol-containing saline was injected through the implanted cannula (0.5 μl at a speed of 0.25 μl/min). The cannula was capped with a blocking stylus, and the mouse was returned to its home cage for 15 min prior to behavioral testing. Each mouse received two days of muscimol and two days of saline injection, with treatment order balanced across animals and data averaged within treatment for analysis.

Induced pupil dilation

The mouse was lightly anesthetized using isoflurane, and a drop of saline (0.9%) or atropine solution (1% atropine in saline) was applied to the right eye. The mouse was allowed to recover in its home cage for 30 minutes prior to behavioral testing.

Optogenetic suppression of cortical activity

Optogenetic experiments were carried out approximately 21 days following virus injection. A multi-mode optical fiber (400 μm diameter, 0.22 NA, ThorLabs) was coupled to a 594 nm diode-pumped solid state laser (Excelsior, Spectra Physics) whose output was first directed through a Pockels Cell (Conoptics) for power adjustment. Power was adjusted to 120-160 mW/mm^2 at the output end of the fiber, checked at the start of each session. The fiber was inserted into the guide cannula so that the tip was just above the pial surface. In half of the trials (set pseudorandomly), the light was turned on 2 s prior to the visual stimulus onset and turned off after 3 s via an electronically gated shutter (Uniblitz). Each animal received 3-4 days of optogenetic suppression sessions, with data combined across days for analysis.

Behavioral Training

For all behavioral experiments, mice were habituated to being head-fixed on the wheel for at least three days prior to the start of training. Each trial started with the onset of the 500 ms visual stimulus (CS). The 50 ms air puff (US) was delivered at 450 ms to co-terminate with the CS. For non-imaging experiments, each training day consisted of 60 CS-US pairings 100% contrast. After demonstrating stable conditioned responses (> 50% correct) for 2-3 consecutive days, mice were moved to the performance phase and 60 CS-US pairings with varying contrasts were presented. Mice that did not learn after 14 days of training (n = 7/46) were excluded from further experiments. For calcium imaging experiments, each day consisted of 78 trials and included 12 CS-only trials at varying contrasts. For all sessions, trials were separated by an exponentially distributed inter-stimulus-interval (ISI) ranging from 18 to 33 s.

Calcium imaging

Imaging experiments were conducted approximately 21 days after virus injection and 12 days after surgical implantation. Imaging was carried out using a resonant scanner-based two-photon microscope (MOM, Sutter Instruments) through a 25x, 1.05 NA objective (Olympus) coupled to a Ti:Sapphire laser (MaiTai DeepSee, Spectra Physics) tuned to 920 nm for GCaMP6s. Emitted light was collected through gallium arsenide phosphide photomultiplier tubes (Hamamatsu). To prevent light contamination from the display monitor, the microscope was enclosed in blackout material that extended to the head-post. Images were acquired using ScanImage 2017 (Vidrio) (Pologruto et al., 2003) at ~30 Hz and a resolution of 256x256 pixels (290x290 μm). Layer 5 PN somata were imaged at ~450-600 μm depth relative to the brain surface, as previously published (Lur et al., 2016). The same field of view was imaged on each day and identified neurons were tracked across sessions.

Ex vivo electrophysiology

Mice (P40-50) expressing ArchT-GFP in either CPn or CSt neurons were generated as described above. Under isoflurane anesthesia, mice were decapitated and coronal slices (300 microns thick) were cut in ice-cold external solution containing (in mM): 100 choline chloride, 25 $NaHCO_3$, 1.25 NaH_2PO_4, 2.5 KCl, 7 $MgCl_2$, 0.5 $CaCl_2$, 15 glucose, 11.6 sodium ascorbate and 3.1 sodium pyruvate, bubbled with 95% O_2 and 5% CO_2. Slices containing V1 were transferred to artificial cerebrospinal fluid (ACSF) containing (in mM): 127 NaCl, 25 $NaHCO_3$, 1.25 NaH_2PO_4, 2.5 KCl, 1 $MgCl_2$, 2 $CaCl_2$ and 15 glucose, bubbled with 95% O2 and 5% CO2. After an incubation period of 30 min at 34°C, the slices were maintained at 22–24°C for at least 20 min before use. Experiments were conducted at room temperature (22–24°C) in a submersion-type recording chamber. Whole-cell recordings were obtained from fluorescently identified CPn or CSt cells using an internal solution containing (in mM): 135 K-Gluconate, 10 HEPES, 4 $MgCl_2$, 4 Na_2ATP, 0.4 NaGTP, 10 sodium creatine phosphate, and 1 EGTA, adjusted to pH 7.3 with KOH. Electrophysiological recordings were made using a Multiclamp 700B amplifier (Molecular Devices), filtered at 4 kHz, and digitized at 10 kHz using acquisition software written in MATLAB (Mathworks) (Pologruto et al., 2003). Cells were recorded in either voltage clamp (−70 mV) or current clamp mode. Light-evoked currents were evoked by delivering light pulses (400 ms, 595 nm, 30-40 mW/mm^2) through the microscope objective which was coupled to a light-emitting diode (M595L3, Thorlabs). To evoke trains of action potentials, cells were injected with depolarizing current pulses (600 ms, 200 pA) through the patch pipette.

QUANTIFICATION AND STATISTICAL ANALYSIS

Details for all statistical analyses, including statistical tests used, exact value of n, what n represents, and precision measures (e.g., mean, SEM) are provided in the Results section and in Table S1. All analyses were carried out using MATLAB. No explicit tests of statistical test assumptions were made as, in most cases (e.g., permutation tests), there are minimal assumptions in the underlying model.

Behavioral analysis and statistics

Eyeblink and pupil videos were analyzed offline using MATLAB. To extract eyelid closure, gray-scale images from a single session were binarized to maximize the contrast between the eye (white) and surrounding fur (black). A region of interest around the eye was manually defined, and the time-varying proportion of white pixels was used as a readout for eye closure. These data were normalized by the 5th and 95th percentile values for each session, resulting in a range of 0 to 1, corresponding to a fully open and fully closed eye, respectively. For each trial, the conditioned response (CR) was defined as the maximum eye closure within 450 ms of the visual stimulus onset (prior to air puff). The response time (RT) was defined by identifying the time after CS onset at which the eyelid closure rate crossed a threshold of 5% per 30 ms. The unconditioned response (UR) was defined as the maximum eye closure within a 500 ms window from the onset of the air puff. Trials were identified as correct if the CR:UR ratio was larger than 10% (see Figure S1). CR:UR values were only analyzed for correct trials. Trials were excluded from analysis if the eye closed > 10% within a 2 s window prior to visual stimulus onset. The average percentage of dropped trials was similar for all animals and did not differ significantly for CPn (9.0 ± 1.0%) versus CSt (10.7 ± 0.7%) cohorts (p = 0.62, Mann-Whitney Test). Spontaneous blinks (> 10% full eye closure) were detected during the inter-stimulus-intervals. Spontaneous blink rate was calculated as the average number of blinks per 450 ms interval to compare with the behavioral analysis window.

To extract pupil size, gray-scale images were binarized (independently from analyses of eyeblink) to maximize the contrast between the pupil (black) and surrounding sclera (white). Pupil size was determined as the time-varying proportion of black pixels in a region of interest covering the eye. Pupil data were normalized by the 5th and 95th percentile values for each session. For each trial, arousal state was determined as the average pupil size during the 2 s prior to visual stimulus onset. Trials were classified into large and small pupil classes using the median value across mice.

To determine running speed, the rotational wheel position data during each session were binned over 100 ms intervals and transformed into velocity. For each trial, average running speed during 2 s prior to visual stimulus onset was measured and classified into high and low classes using a threshold of 1 cm/s.

All trials across days from the performance phase (using varied contrast) were concatenated for analysis. Group performance was calculated by averaging the % correct at each contrast across animals and curve fitting these values with a hyperbolic ratio function:

$$\%\ Correct = baseline + \frac{R_{max} \times Contrast^{Power}}{Contrast^{Power} + c_{50}^{Power}}$$

For fitting purposes, baseline was the spontaneous blink rate at 0% contrast, c50 was restricted to < 50% contrast, and the power was restricted to between 1 and 3. In the present work, we limited statistical analyses of behavioral performance to the calculated R_{Max} value. Contrast dependence of both the CR:UR ratio and the RT were fit with linear functions for contrast values above 2%.

To address whether behavioral variables (e.g., R_{Max}, CR:UR ratio, RT) varied by muscimol treatment, arousal, or optogenetic manipulation, we then conducted a stratified permutation analysis to maximize the use of data points across contrast levels and allow pairwise comparisons between conditions within each mouse. Trials within mouse at a single contrast level were regarded as a stratum. For each permutation, condition labels (e.g., muscimol versus saline) were randomly permuted (shuffled) within each strata so that the number of trials per condition per contrast per animal remained unchanged. The performance at various contrast levels across all mice was then averaged using the permuted data and the population averages were then fit with the appropriate curve (hyperbolic ratio or linear) for the two paired conditions. We then calculated the ratio of the parameter of interest (e.g., R_{Max}) from these curves. This process was repeated 10,000 times to generate a null distribution for the group average parameter. The p value for each parameter was calculated by summing the proportion of points beyond the actual value in the null distribution.

This permutation approach maximizes power but requires curve fitting of data and does not allow for a simple, paired statistical comparison. Therefore, to complement our analyses we carried out a direct pairwise test of parameter values across mice using data from trials at 100% contrast. The statistical results did not differ in any case between the two methods. Permutation results are presented in the Main text, while all results (Permutation and Pairwise) are provided in Table S1.

Imaging analysis and statistics

Ca^{2+} imaging data were motion-corrected using the Moco plugin for ImageJ (Dubbs et al., 2016), taking the first 200 frames of each movie as the template. Subsequent analyses were carried out using MATLAB. Videos from successive days were translated onto the first-day template. Regions of interest were selected as previously described (Chen et al., 2013b). Fluorescence (F) over time was measured by averaging all pixels in a given ROI, and the contamination from the surrounding neuropil was removed as previously described with a discounting coefficient of 0.70 (Chen et al., 2013b; Lur et al., 2016). ΔF/F was calculated as $(F\text{-}F_0)/F_0$, where F_0 was the lowest 10% of values from the neuropil-subtracted trace for each session.

The visual response of a neuron on a given trial was defined as the mean ΔF/F in a 300ms window after the visual stimulus onset, subtracting the mean ΔF/F over the 300 ms preceding the stimulus. A neuron was classified as visually responsive if its response at 100% contrast was significantly larger than those at 0% contrast using a one-sided Student's t test. Only visually responsive neurons were included in the analyses unless otherwise noted.

The contrast response function (CRF) of each visually responsive neuron was estimated using a 3-parameter rectified linear unit function (ReLU), as it yielded the largest R-square and the smallest adjusted root-mean-squared-error compared to sigmoidal fit (Figure S4):

$$\Delta\mathbf{F}/\mathbf{F} = offset + \log_{10}(\mathbf{Contrast}) \times Slope \times \mathrm{I}(\mathbf{Contrast} > Threshold)$$

where offset is the spontaneous calcium activity at 0% contrast and slope indicates how fast the visual response increases with contrast, only when contrast is above threshold. The average visual response amplitudes, per contrast, of all the visually responsive neurons in each animal were grouped to generate a within animal CRF, fitted as described above. The coefficient of variation (standard deviation divided by mean) versus contrast was plotted similarly. Pairwise noise correlations between visually responsive neurons were calculated after Z-scoring response amplitudes across trials and concatenating across all trials. Noise correlations were defined as the Pearson's r-value across trials for each pair of cells. A modulation index for locomotion was calculated for each neuron as:

$$MI = \left(Slope_{High} - Slope_{Low}\right) / \left(Slope_{High} + Slope_{Low}\right)$$

For calcium imaging experiments, data from all visually responsive neurons within an animal were pooled for calculation of across-animal statistics. This approach is more conservative than an across-cells comparison which violates independency assumptions for

most tests. As the animal numbers were small (n = 6 for CPn neurons and n = 6 for CSt neurons), we used non-parametric analyses, specifically Mann-Whitney U Tests for non-paired samples and Wilcoxon tests for paired samples.

To quantify the relationship of neuronal activity to behavior, trials were classified into correct and incorrect, and analyzed via permutation, as described above. The trial-by-trial decoder was built to predict the behavioral performance of individual animals using visually evoked activity via simple logistic regression as follows. Let x_i be a vector of visual responses for each trial for the i-th neuron, p is the probability of a correct trial, and m is the total number of recorded neurons in a mouse:

$$log\frac{p}{1-p} = \beta_0 + \sum_{i=1}^{m} \beta_i x_i$$

Coefficients were estimated using maximum likelihood from 90% of trials and used to predict the 10% of the trials (10-fold cross-validation). A predicted trial was regarded as correct for $p >= 0.5$. The predicted psychometric performance was then plotted against contrast using the actual contrast labels. For these logistic regression analyses, we accounted for unbalanced numbers of neurons in the two subpopulations. Each mouse in the CPn cohort was matched with a mouse in the CSt cohort and an equally sized subset of neurons was randomly selected for each pair. For each mouse, this selection process was repeated 15,000 times or the maximum combination of neurons, whichever was smaller. This balancing was only used for the predictive modeling analyses.

The performance of each population to predict behavior was measured as a d' value, defined as: Z(model hit rate)-Z(model false alarm rate), where the function Z(p) with $p \in [0,1]$ is the inverse cumulative distribution function of a standard Gaussian distribution. A similar approach was used for constructing a single neuron decoder. A two-sample t test was used to compare the cell-wise performance between subpopulations.

To compare our results with a more conservative measure of neuronal response, we also carried out similar analyses where the neuronal response on a single trial was limited to the time window after stimulus onset but preceding the blink. As the duration of this period varies across trials, we defined the visual response as the slope during this period after subtracting the slope during the preceding baseline period. Finally, to address the role of within trial correlations between cells, we carried out a similar logistic regression analysis after randomly shuffling trials within specified contrast levels.

DATA AND CODE AVAILABILITY

The datasets and code supporting the current study have not been deposited in a public repository due to file size constraints but are available from the corresponding author on reasonable request.